Microscopic analysis of charge and spin photocurrents injected by circularly polarized one-color laser pulses in GaAs quantum wells

Huynh Thanh Duc, Jens Förstner, and Torsten Meier
Department Physik and Center for Optoelectronics and Photonics Paderborn (CeOPP), Universität Paderborn, Warburger Str. 100, D-33098 Paderborn, Germany
(Received 19 July 2010; published 21 September 2010)

The dynamics of charge and spin injection currents excited by circularly polarized, one-color laser beams in semiconductor quantum wells is analyzed. Our microscopic approach is based on a 14×14 $k\cdot p$ band-structure theory in combination with multisubband semiconductor Bloch equations which allows a detailed analysis of the photogenerated carrier distributions and coherences in k space. Charge and spin injection currents are numerically calculated for [110]- and [001]-grown GaAs quantum wells including dc population contributions and ac contributions that arise from intersubband coherences. The dependencies of the injection currents on the excitation conditions, in particular, the photon energy are computed and discussed.

DOI: 10.1103/PhysRevB.82.115316 PACS number(s): 78.67.De, 73.63.Hs, 78.47.J−, 72.25.Fe

I. INTRODUCTION

The ultrafast coherent generation of charge and spin injection currents with one- and two-color laser excitation has received significant attention recently.[1–31] Both excitation schemes allow one to generate charge and spin currents on femtosecond time scales and promise applications in ultrafast optoelectronics and spintronics. The two-color current generation process uses the interference of one- and two-photon excitations, and is a third-order nonlinear optical process that does not rely on the material symmetry or details of the band structure.[2–4,7,12–17,20,25,26,28–30]

One-color injection currents however arise from a spin splitting of the energy bands in systems of reduced symmetry and are of second order in the light field, i.e., the currents are proportional to the light intensity. Since this current is maximal for circularly polarized excitation, it is referred to as circular photogalvanic effect.[1,8–10] For linearly polarized excitation, interband transitions are accompanied by asymmetrical interatomic shifts of electrons in real space which result in the so-called shift current.[1,5,21–23] In the present paper we focus on the generation of injection currents and neglect the shift currents. Most of the calculations presented below are carried out for circularly polarized excitations where the shift current vanishes.

Injection currents do not exist in bulk GaAs which has a T_d point group symmetry, however, they occur in GaAs quantum wells (QWs) of reduced symmetry. A theoretical approach to the spin-splitting-induced photogalvanic effect for GaAs QWs has been presented by Golub.[11] The spin splitting has been introduced via Dresselhaus and Rashba[11] terms and the photon energy dependence of the injected charge current for [001]-grown QWs has been calculated. Here, we present a microscopic approach which includes the spin splitting arising from the inversion asymmetry of the material via 14×14 $k\cdot p$ band-structure calculations.[32–38] The resulting anisotropic and spin-split electronic bands and wave functions are used to set up multisubband semiconductor Bloch equations (SBE),[39,40] i.e., the equations of motion for the intersubband and intersubband coherences and the electron populations. By limiting these equations to the second order in the light-matter interaction and solving them, it is possible to obtain the injection current tensor which is used in macroscopic approaches to current generation. Via numerical solutions of the multisubband SBE we obtain the time-dependent charge and spin injection currents arising from populations and intersubband coherences. Our microscopic approach provides a detailed description of the current generation process and allows to disentangle how strongly different bands and transitions contribute to the injection currents. The multisubband SBE include Coulomb many-body effects in time-dependent Hartree-Fock approximation and are thus capable of describing excitonic effects which are known to influence one- and two-color injection currents.[15,16,24,30] Since the injection charge currents generated by circularly polarized one-color excitation are spin polarized,[9,27] they are accompanied by spin currents. These spin currents are also described by our multisubband SBE and analyzed below.

In Sec. II we explain our microscopic approach that is based on 14×14 $k\cdot p$ band-structure theory in combination with multisubband SBE which allows a detailed analysis of the dynamics of the photogenerated carrier distributions and coherences. Using this theory, charge and spin injection currents for GaAs/$Al_xGa_{(1-x)}As$ QW systems grown in [110] and [001] directions that are generated by the excitation with femtosecond one-color laser pulses are computed and discussed in Sec. III. The main results are briefly summarized in Sec. IV.

II. THEORETICAL APPROACH

In this section, we outline our theoretical approach which is used for the numerical calculations of charge and spin injection currents by femtosecond laser pulses that are presented in Sec. III.

A. Quantum-well band structure

We start by determining the electronic band structure and wave functions of the considered QW systems using 14×14 band $k\cdot p$ theory.[35] The electron wave functions are de-

scribed in envelope function approximation. Choosing z as the growth direction of the QW, the wave functions are written as $\Psi_{\mathbf{k}_\parallel}(\mathbf{r})=e^{i\mathbf{k}_\parallel\mathbf{r}_\parallel}\Sigma_n f_{n\mathbf{k}_\parallel}(z)u_n(\mathbf{r})$. Here, $\mathbf{k}_\parallel$ is the in-plane wave vector, $u_n(\mathbf{r})$ are band-edge Bloch functions, and $f_{n\mathbf{k}_\parallel}(z)$ are slowly varying envelope functions which satisfy the effective-mass equation

$$\sum_{m=1}^{14}[H_{nm}(\mathbf{k}_\parallel,-i\partial_z)+V_n(z)\delta_{nm}]f^{\lambda}_{m\mathbf{k}_\parallel}(z)=E^{\lambda}_{\mathbf{k}_\parallel}f^{\lambda}_{n\mathbf{k}_\parallel}(z). \quad (1)$$

In Eq. (1), $H(\mathbf{k})$ is the 14×14 bulk Hamiltonian and $V(z)$ is the QW potential.[35] The Hamiltonians describing various crystallographic directions of the z axis are derived by Euler rotations of the coordinate system. Since the basis functions of the 14-band $k\cdot p$ model are defined by 1/2 and 3/2 angular momentum eigenfunctions, the unitary rotation operators $\mathfrak{D}^{(1/2)}$ and $\mathfrak{D}^{(3/2)}$ can be applied.[41]

To solve Eq. (1) we follow Ref. 35 using the Löwdin perturbation theory to block diagonalize the 14×14 bulk Hamiltonian into blocks of 2×2 and 4×4 elements for the Γ_{6c}-conduction bands and the Γ_{8v}-valence bands, respectively.[38] Then, the electronic wave functions and energies are computed from the effective-mass equation for the obtained Hamiltonian blocks by applying the variational calculation described in Ref. 42.

The bulk band parameters of GaAs and $Al_xGa_{(1-x)}As$ materials used in our calculations are taken from Ref. 35 and the temperature dependence of the band gap is described by the Varshni relation $E_g(T)=E_g(0)-\alpha T^2/(T+\beta)$. The nonparabolic and anisotropic band structures computed for [001]- and [110]-grown 12-nm-thick GaAs/$Al_{0.35}Ga_{0.65}As$ QW systems at room temperature $T=300$ K are shown in Fig. 1. Due to the inversion asymmetry of GaAs lattice structure a small spin splitting of the electronic bands is obtained which is responsible for the generation of the injection currents. We notice that for the [001]-grown QW a small spin splitting exists for all directions of $\mathbf{k}_\parallel$ while for the [110]-grown QW the spin splitting is quite large when $\mathbf{k}_\parallel$ is parallel to $[\bar{1}10]$ and vanishes when $\mathbf{k}_\parallel$ is parallel to $[00\bar{1}]$.

B. Multisubband semiconductor Bloch equations

Here, we describe the derivation of the multisubband SBE which are used to compute the charge and spin injection currents in Sec. III. In the multisubband SBE we consider the 14×14 band $k\cdot p$ band structure and use 14×14 band $k\cdot p$ wave functions in the evaluation of the optical and Coulomb matrix elements.

The Hamiltonian that is considered for the analysis of the ultrafast optical response of the QW systems consists of three contributions[28,37–40]

$$\hat{H}=\hat{H}_{\text{band structure}}+\hat{H}_{\text{light matter}}+\hat{H}_{\text{Coulomb}}. \quad (2)$$

The single-particle Hamiltonian for noninteracting Bloch electrons is given by

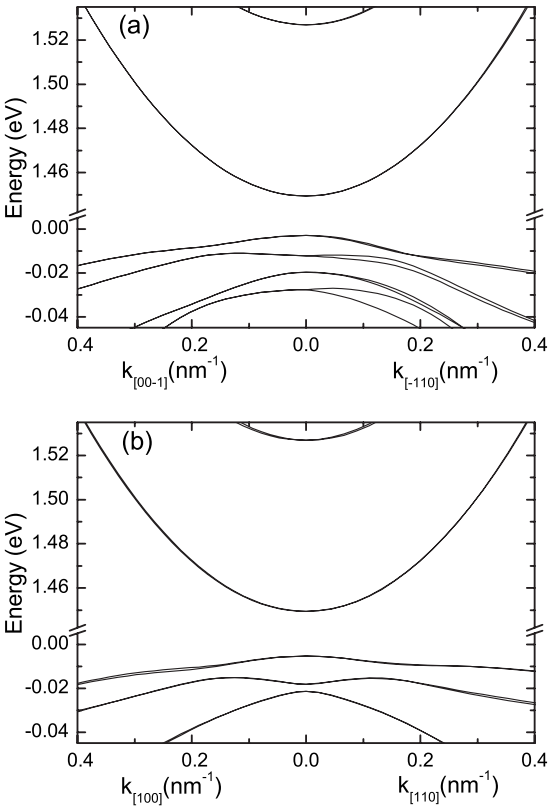

FIG. 1. Band structure of GaAs/$Al_{0.35}Ga_{0.65}As$ QW systems with 12-nm-wide wells grown in the directions (a) [110] and (b) [001]. The band-gap energies for these two QWs are 1.453 eV and 1.455 eV, respectively.

$$\hat{H}_{\text{band structure}}=\sum_{\lambda\mathbf{k}_\parallel}E^{\lambda}_{\mathbf{k}_\parallel}a^{\dagger}_{\lambda\mathbf{k}_\parallel}a_{\lambda\mathbf{k}_\parallel}. \quad (3)$$

Here, $E^{\lambda}_{\mathbf{k}_\parallel}$ is the electronic dispersion taken from the 14×14 band $k\cdot p$ calculations and $a^{\dagger}_{\lambda\mathbf{k}_\parallel}(a_{\lambda\mathbf{k}_\parallel})$ is the creation (annihilation) operator of an electron with wave vector $\mathbf{k}_\parallel$ in the band λ. The light-matter interaction is described by the minimal coupling Hamiltonian in the velocity gauge

$$\hat{H}_{\text{light matter}}=\frac{e}{m_0}\mathbf{A}(t)\cdot\sum_{\lambda\lambda'\mathbf{k}_\parallel}\mathbf{\Pi}^{\lambda\lambda'}_{\mathbf{k}_\parallel}a^{\dagger}_{\lambda\mathbf{k}_\parallel}a_{\lambda'\mathbf{k}_\parallel}, \quad (4)$$

where $\mathbf{A}(t)$ is the vector potential of the light field and $\mathbf{\Pi}^{\lambda\mu}_{\mathbf{k}_\parallel}$ are momentum matrix elements, which are evaluated using the 14×14 band $k\cdot p$ wave functions

$$\mathbf{\Pi}^{\lambda\lambda'}_{\mathbf{k}_\parallel}=\int dz\sum_{mn}f^{\lambda*}_{m\mathbf{k}_\parallel}(z)\pi_{mn}(\mathbf{k}_\parallel,-i\partial_z)f^{\lambda'}_{n\mathbf{k}_\parallel}(z) \quad (5)$$

with $\pi_{nm}(\mathbf{k})=\frac{m_0}{\hbar}\nabla_{\mathbf{k}}H_{nm}(\mathbf{k})$. The many-body Coulomb interaction is described by

$$\hat{H}_{\text{Coulomb}} = \frac{1}{2} \sum_{\lambda_1\lambda_2\lambda_3\lambda_4 \mathbf{k}_\parallel \mathbf{k}'_\parallel \mathbf{q}_\parallel} V^{\lambda_1\lambda_2\lambda_3\lambda_4}_{\mathbf{k}_\parallel,\mathbf{k}'_\parallel,\mathbf{q}_\parallel} \times a^\dagger_{\lambda_1 \mathbf{k}_\parallel+\mathbf{q}_\parallel} a^\dagger_{\lambda_2 \mathbf{k}'_\parallel-\mathbf{q}_\parallel} a_{\lambda_3 \mathbf{k}'_\parallel} a_{\lambda_4 \mathbf{k}_\parallel}, \tag{6}$$

where the Coulomb matrix elements read

$$V^{\lambda_1\lambda_2\lambda_3\lambda_4}_{\mathbf{k}_\parallel,\mathbf{k}'_\parallel,\mathbf{q}_\parallel} = \frac{e^2}{2\epsilon\epsilon_0 L^2 |\mathbf{q}_\parallel|} \int dz_1 \int dz_2 e^{-|\mathbf{q}_\parallel||z_2-z_1|} \times \sum_m f^{\lambda_1 *}_{m\mathbf{k}_\parallel+\mathbf{q}_\parallel}(z_1) f^{\lambda_4}_{m\mathbf{k}_\parallel}(z_1) \sum_n f^{\lambda_2 *}_{n\mathbf{k}'_\parallel-\mathbf{q}_\parallel}(z_2) f^{\lambda_3}_{n\mathbf{k}'_\parallel}(z_2). \tag{7}$$

The dynamical optoelectronic response is analyzed using the Heisenberg equation of motion for the expectation values $\mathrm{x}^{\lambda\lambda'}_{\mathbf{k}_\parallel} = \langle a^\dagger_{\lambda \mathbf{k}_\parallel} a_{\lambda' \mathbf{k}_\parallel} \rangle$. The band indices λ and λ' refer to the conduction subbands c, c' and the valence subbands v, v'. $\mathrm{x}^{\lambda\lambda'}_{\mathbf{k}_\parallel}$ represents either an interband coherence ($p^{vc}_{\mathbf{k}_\parallel}$), an intersubband coherences ($n^{cc'}_{\mathbf{k}_\parallel}$ and $n^{vv'}_{\mathbf{k}_\parallel}$, where $c \neq c'$ and $v \neq v'$), or a population ($n^{cc}_{\mathbf{k}_\parallel}$ and $n^{vv}_{\mathbf{k}_\parallel}$). Evaluating the Heisenberg equations of motion and treating the many-body Coulomb interaction in the time-dependent Hartree-Fock approximation[39,40] we obtain the multisubband SBE as[38]

$$\frac{\partial}{\partial t} \mathrm{x}^{\lambda\lambda'}_{\mathbf{k}_\parallel} = \frac{i}{\hbar}(E^\lambda_{\mathbf{k}_\parallel} - E^{\lambda'}_{\mathbf{k}_\parallel}) \mathrm{x}^{\lambda\lambda'}_{\mathbf{k}_\parallel} + \frac{i}{\hbar} \sum_\mu [\Omega^{\mu\lambda}_{\mathbf{k}_\parallel} \mathrm{x}^{\mu\lambda'}_{\mathbf{k}_\parallel} - \Omega^{\lambda'\mu}_{\mathbf{k}_\parallel} \mathrm{x}^{\lambda\mu}_{\mathbf{k}_\parallel}] + \frac{\partial}{\partial t} \mathrm{x}^{\lambda\lambda'}_{\mathbf{k}_\parallel}\Big|_{\text{coll}} \tag{8}$$

with

$$\Omega^{\lambda\lambda'}_{\mathbf{k}_\parallel} = \frac{e}{m_0} \mathbf{A}(t) \cdot \mathbf{\Pi}^{\lambda\lambda'}_{\mathbf{k}_\parallel} - \sum_{\mu\nu\mathbf{q}_\parallel} V^{\mu\lambda\nu\lambda'}_{\mathbf{k}_\parallel,\mathbf{k}_\parallel+\mathbf{q}_\parallel,\mathbf{q}_\parallel} x^{\mu\nu}_{\mathbf{k}_\parallel+\mathbf{q}_\parallel}. \tag{9}$$

For $\lambda \neq \lambda'$, $\Omega^{\lambda\lambda'}_{\mathbf{k}_\parallel}$ is the renormalized Rabi frequency whereas for $\lambda = \lambda'$ it describes the renormalization of the energy bands. The term $\frac{\partial}{\partial t} \mathrm{x}^{\lambda\lambda'}_{\mathbf{k}_\parallel}|_{\text{coll}}$ denotes collision contributions originating from scattering processes. Since the microscopic details of these effects are not relevant for the qualitative features analyzed here and in order to keep the numerical effort within reasonable limits, dephasing, and relaxation are treated on a phenomenological level. The dephasing of interband and intersubband coherences is modeled by $\frac{\partial}{\partial t} x^{\lambda\lambda'}_{\mathbf{k}_\parallel}|_{\text{coll}} = -x^{\lambda\lambda'}_{\mathbf{k}_\parallel}/\tau_2$ and the relaxation of populations toward quasiequilibrium distributions within respective band is described by $\frac{\partial}{\partial t} n^{\lambda\lambda}_{\mathbf{k}_\parallel}|_{\text{coll}} = -[n^{\lambda\lambda}_{\mathbf{k}_\parallel} - n^{\text{FD}}_{\lambda\mathbf{k}_\parallel}(T)]/\tau_1$, where $n^{\text{FD}}_{\lambda\mathbf{k}_\parallel}(T)$ is the Fermi-Dirac distribution at temperature T. In our calculations, we use dephasing and relaxation times of $\tau_2 = \tau_1 = 150$ fs, which are typical values for the QW system and excitation conditions considered here.[17]

C. Charge and spin currents

By numerically solving Eqs. (8) we obtain the time-dependent carrier populations ($n^{vv}_{\mathbf{k}_\parallel}$ and $n^{cc}_{\mathbf{k}_\parallel}$) and intersubband ($n^{v'v}_{\mathbf{k}_\parallel}$ and $n^{c'c}_{\mathbf{k}_\parallel}$) as well as interband ($p^{vc}_{\mathbf{k}_\parallel}$) coherences. The injection currents are determined by the populations and the intersubband coherences. We distinguish here between the contributions of these terms to the injection currents and define the population charge current

$$\mathbf{J}^{\text{pop}}(t) = \frac{e}{m_0} \sum_{c,\mathbf{k}_\parallel} \mathbf{\Pi}^{cc}_{\mathbf{k}_\parallel} n^{cc}_{\mathbf{k}_\parallel} + \frac{e}{m_0} \sum_{v,\mathbf{k}_\parallel} \mathbf{\Pi}^{vv}_{\mathbf{k}_\parallel} n^{vv}_{\mathbf{k}_\parallel} \tag{10}$$

and the coherent charge current

$$\mathbf{J}^{\text{coh}}(t) = \frac{e}{m_0} \sum_{c \neq c',\mathbf{k}_\parallel} \mathbf{\Pi}^{cc'}_{\mathbf{k}_\parallel} n^{c'c}_{\mathbf{k}_\parallel} + \frac{e}{m_0} \sum_{v \neq v',\mathbf{k}_\parallel} \mathbf{\Pi}^{vv'}_{\mathbf{k}_\parallel} n^{v'v}_{\mathbf{k}_\parallel}. \tag{11}$$

The total charge current $\mathbf{J}$ is the sum over the population and the coherent terms, i.e., $\mathbf{J}(t) = \mathbf{J}^{\text{pop}}(t) + \mathbf{J}^{\text{coh}}(t)$. The electron or hole contributions to the injection current can be computed separately by restricting the band summations in Eqs. (10) and (11) to only the conduction or valence band indices, respectively.

Analogously, the population and coherent spin currents for the projection of the spin in i direction ($i = x, y, z$) is defined by

$$\mathbf{S}^{\text{pop}}_i(t) = \frac{\hbar}{m_0} \sum_{c,\mathbf{k}_\parallel} \Sigma^{cc}_{i\mathbf{k}_\parallel} \mathbf{\Pi}^{cc}_{\mathbf{k}_\parallel} n^{cc}_{\mathbf{k}_\parallel} + \frac{\hbar}{m_0} \sum_{v,\mathbf{k}_\parallel} \Sigma^{vv}_{i\mathbf{k}_\parallel} \mathbf{\Pi}^{vv}_{\mathbf{k}_\parallel} n^{vv}_{\mathbf{k}_\parallel} \tag{12}$$

and

$$\mathbf{S}^{\text{coh}}_i(t) = \frac{\hbar}{m_0} \sum_{c \neq c',\mathbf{k}_\parallel} \Sigma^{cc'}_{i\mathbf{k}_\parallel} \mathbf{\Pi}^{c'c}_{\mathbf{k}_\parallel} n^{cc'}_{\mathbf{k}_\parallel} + \frac{\hbar}{m_0} \sum_{v \neq v',\mathbf{k}_\parallel} \Sigma^{vv'}_{i\mathbf{k}_\parallel} \mathbf{\Pi}^{v'v}_{\mathbf{k}_\parallel} n^{vv'}_{\mathbf{k}_\parallel}, \tag{13}$$

respectively. The projection of the spin in i direction is described by the angular momentum matrix elements[35]

$$\Sigma^{cc'}_{i\mathbf{k}_\parallel} = \frac{1}{2} \int dz \sum_{mn} f^{c*}_{m\mathbf{k}_\parallel}(z) \sigma_i f^{c'}_{n\mathbf{k}_\parallel}(z) \tag{14}$$

and

$$\Sigma^{vv'}_{i\mathbf{k}_\parallel} = \int dz \sum_{mn} f^{v*}_{m\mathbf{k}_\parallel}(z) \mathcal{J}_i f^{v'}_{n\mathbf{k}_\parallel}(z), \tag{15}$$

where σ_i are the Pauli matrices and $\mathcal{J}_i$ the spin-3/2 matrices, respectively. The total spin current $\mathbf{S}$ is the sum over the population and the coherent contributions, i.e., $\mathbf{S}(t) = \mathbf{S}^{\text{pop}}(t) + \mathbf{S}^{\text{coh}}(t)$. The electron or hole contributions to the injected spin current can be computed separately by restricting the band summations in Eqs. (12) and (13) to only the conduction or valence band indices, respectively.

III. NUMERICAL RESULTS

In this section, we present numerical results on charge and spin injection currents for QW systems grown in [110] and [001] direction that are obtained by solving the multisubband SBE. In our numerical solutions of the multisubband SBE we include the two energetically lowest conduction bands (e1 and e2) and four energetically highest valence bands (hh1, hh2, lh1, and hh3). Here, hh and lh denotes whether the

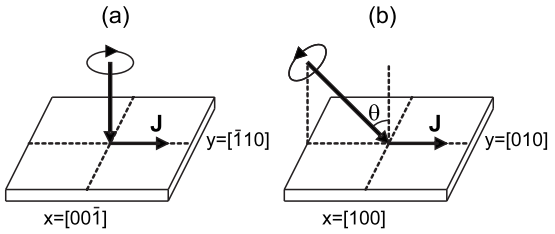

FIG. 2. The geometry of the optical excitation of QW systems grown in (a) [110] and (b) [001] directions. Whereas in [110] QWs injection currents can be generated with normal incidence in [001] QWs the excitation has to be tilted by a finite angle Θ to generate injection currents.

wave functions of the valence bands at $\mathbf{k}_{\|}=0$ contain heavy-hole or light-hole states. Each of these bands consists of two spin-split branches, i.e., there are totally twelve bands taken into account. Due to the large number of bands as well as the anisotropy of the two-dimensional dispersion the numerical evaluation of the Coulomb matrices is very costly and also the integration of the multisubband SBE with Hartree-Fock renormalizations requires a significant amount of computer memory and time. We therefore neglect excitonic effects in most of calculations. Since excitonic effects are strong near the band gap, this approximation is reasonable for excitations well above the band gap.[15,16,28] That our approach is able to describe the influence of excitonic effects on injection currents is shown in Fig. 7. We find an enhanced current generation for excitation of the hh- and lh-exciton resonances, and the expected decrease of excitonic effects for higher excitation frequencies. A more detailed analysis of the influence of excitonic effects on the generation of injection currents in QWs will be presented elsewhere.

A. Charge current

1. [110]-grown QWs

As shown in Fig. 2(a), we use normal incidence in our analysis of charge and spin injection currents for [110]-grown QWs. The laser pulse with central frequency ω used in the solutions of the multisubband SBE is given by

$$\mathbf{E}(t) = E_0 e^{-(t/\tau_L)^2} e^{i\omega t}(1, e^{i\phi}, 0) + \text{c.c.}, \tag{16}$$

where E_0 is the amplitude and ϕ is the relative phase between the x and y components of the field. The light pulse has a Gaussian envelope with a duration τ_L. For our calculations we take $\tau_L=150$ fs and $E_0=4.5\times10^4$ V/cm which produces a density of photoinduced carriers of about 10^{11} cm^{-2}.

The numerical solutions of the multisubband SBE show that for circularly polarized fields the optical excitation produces asymmetric distributions of spin polarized carriers in k space, which results in nonvanishing charge currents flowing in the direction $[\bar{1}10]$.[31] Time-dependent charge currents J^{pop} and J^{coh} for various polarizations of the light field are shown in Figs. 3(a) and 3(b). During the excitation with the laser pulse, the charge currents are generated, rise, and have a maximum near the end of the pulse at approximately $t=100$ fs. The relaxation of populations and dephasing of coherences leads to an exponential decay of the charge currents for longer times. The ϕ dependence of population current is given by $J^{\text{pop}} \propto \sin(\phi)$ (Ref. 8) and therefore J^{pop} maximizes for circularly polarized excitations ($\phi=\pi/2, 3\pi/2$) and vanishes for linearly polarized excitations ($\phi=0, \pi$). Unlike the population current, the coherent current J^{coh} is an alternating current, see Fig. 3(b), which oscillates with frequencies and amplitudes determined by the intersubband coherence. For a simple multilevel model, the intersubband coherence has the form $n^{\lambda\lambda'} \propto \exp(-\frac{\omega_{\lambda\lambda'}^2}{4\delta\omega^2})\exp(-i\omega_{\lambda\lambda'}t)$, where $\omega_{\lambda\lambda'}$ is intersubband transition frequency and $\delta\omega=1/\tau_L$. Since for the considered laser pulse duration and QW systems, the energy difference between conduction subbands $\omega_{cc'}$ is much larger than $\delta\omega$, the electron contribution to the coherent current is negligible and hence, the overall coherent current is dominated by hole intersubband coherences. Figure 3(b) demonstrates that the phase difference ϕ changes the phase of the current oscillations. Therefore, unlike the population charge current the coherent charge current J^{coh} exists even for linearly polarized excitations ($\phi=0, \pi$).

Figure 4 shows the dependence of the charge current J^{pop} at time $t=100$ fs on the photon energy for excitation with

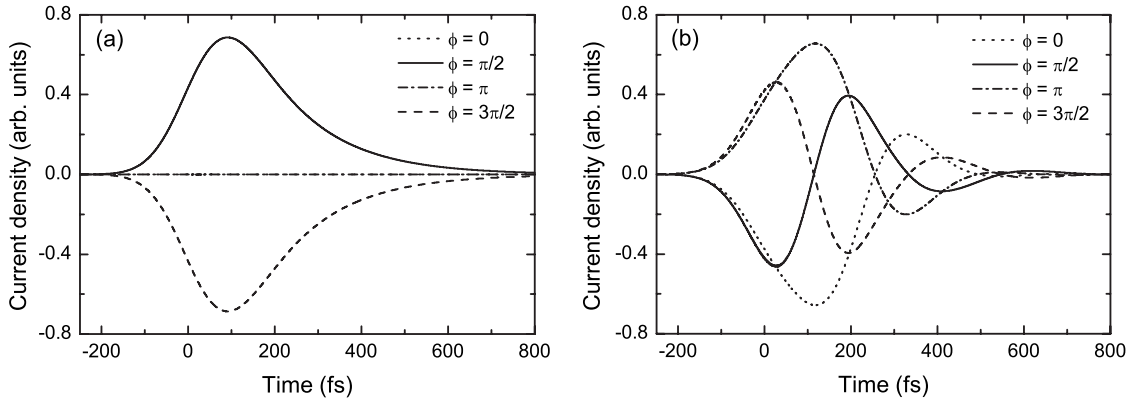

FIG. 3. Time-dependent charge currents from (a) the populations J^{pop} and (b) the intersubband coherences J^{coh} for various polarizations of the incident pulse for a [110]-grown GaAs/$Al_{0.35}Ga_{0.65}As$ QW system with a 12-nm-wide well. The excitation pulses have a central photon energy of $\hbar\omega=1.501$ eV, a duration of $\tau_L=150$ fs, and an amplitude of $E_0=4.5\times10^4$ V/cm.

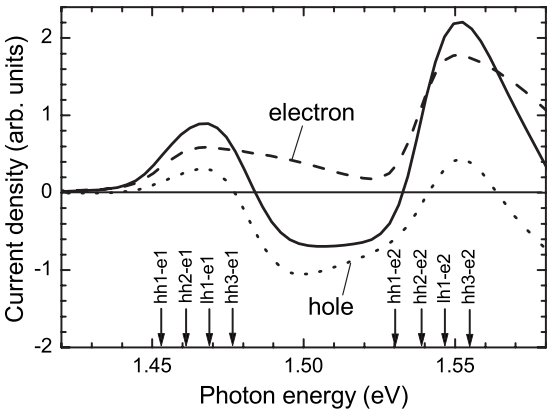

FIG. 4. Photon-energy dependence of the population charge current J^{pop} at $t=100$ fs for a [110]-grown GaAs/$Al_{0.35}Ga_{0.65}As$ QW system with a 12-nm-wide well. Shown is the total current J^{coh} (solid line) and the electron (dashed line) and hole currents (dotted line). The vertical arrows highlight the photon energies that correspond to different interband transitions at $\mathbf{k}_{\parallel}=0$.

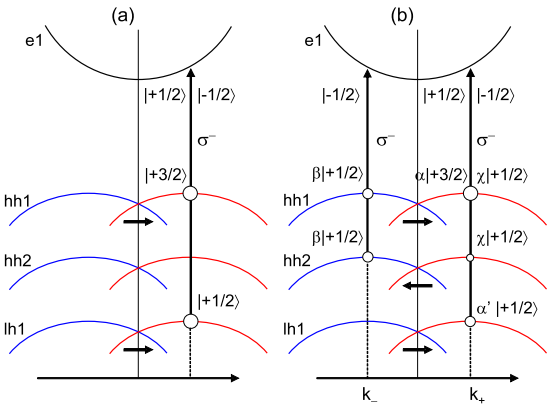

FIG. 5. (Color online) This scheme illustrates the influence of band mixing on the hole current direction. The hole currents J^{pop} in different valence bands are generated by σ^--polarized excitations. (a) Without hh-lh band mixing: the hh2-e1 transition is forbidden leading to a vanishing current in hh2 band. Due to the optical selection rules the hole currents generated in the hh1 and the lh1 flow in the same direction. (b) With hh-lh band mixing: the optical selection rules lead to the opposite direction of the current in the hh2 band compared to the currents in the hh1 and the lh1 bands.

circularly polarized light fields ($\phi=\pi/2$). The total current (solid line) consists of the electron current (dashed line) and the hole current (dotted line). Since holes are heavier than electrons one could expect that the hole current contribution is small and the injection current is mainly caused by electrons. However, as is shown in Fig. 1(a), the valence bands have a larger spin splitting than conduction bands, which leads to a stronger asymmetry of the k-space distribution of holes than electrons. In our calculations these two effects strongly compensate and therefore we obtain comparable strengths of the hole and electron currents.[31] The main difference between the hole and the electron currents is that the hole current reverses its direction when the photon energy is increased. This finding can be explained by the presence of valence band mixing.

A schematic illustration of the generation of hole injection currents J^{pop} in different valence bands by σ^--polarized excitation is shown in Fig. 5. Without band mixing, the optical selection rules lead to currents in the e1, hh1, and lh1 bands that all flow into the positive direction, see Fig. 5(a), and the directions remain unchanged as function of the photon energy.[31] With hh-lh band mixing, the hole wave function is a linear combination of hh and lh wave functions. Let us assume that the heavy-holelike wave functions for the upper spin-split branch at $\pm k$ have the form

$$\psi_{\pm}^{hh}(\pm k) = \alpha(\pm k)\left|\pm\frac{3}{2}\right\rangle + \beta(\pm k)\left|\mp\frac{1}{2}\right\rangle + \chi(\pm k)\left|\pm\frac{1}{2}\right\rangle. \tag{17}$$

Due to the time reversal symmetry we have $|\alpha(+k)|^2=|\alpha(-k)|^2$, $|\beta(+k)|^2=|\beta(-k)|^2$, and $|\chi(+k)|^2=|\chi(-k)|^2$. Near the band edge, typically, we also have $|\alpha|^2>|\beta|^2>|\chi|^2$. It can be seen from the Fig. 5(b) that the transition from hh1 to e1 bands leads to a hole population which is proportional to $|\alpha|^2+|\chi|^2$ at k_+ and $|\beta|^2$ at k_-. This results in a current in the direction of positive k. Since the hh component is dark in the hh2-e1 transition, the hole population in hh2 band are larger at k_- ($|\beta|^2$) than at k_+($|\chi|^2$) and therefore the current flows into the negative direction. The light-holelike wave functions that describe holes in the third valence band can similarly be written as

$$\psi_{\pm}^{lh}(\pm k) = \alpha'(\pm k)\left|\pm\frac{1}{2}\right\rangle + \beta'(\pm k)\left|\mp\frac{3}{2}\right\rangle + \chi'(\pm k)\left|\pm\frac{3}{2}\right\rangle. \tag{18}$$

Because the hh component is dark in the lh1-e1 transition, the hole current is caused only by the light hole content and thus flows in the positive direction. In the detailed calculation, presented in Ref. 31, the hole currents in the hh2 and the hh3 bands flow in the opposite directions compared to the currents in the hh1 and the lh1 bands. The oppositely oriented currents being excited in different valence subbands result in an oscillatory dependence of the total population charge current J^{pop} on the photon energy. The computed excitation-frequency dependence of the population charge current J^{pop} magnitude and direction obtained within our approach has been shown to be in good agreement with experimental results.[31]

Numerical results for the dependence of the relative phase and the peak to peak amplitude of the alternating coherent current J^{coh} on the photon energy are shown in Figs. 6(a) and 6(b). The peak to peak amplitude is the difference between the maximum and minimum of $J^{coh}(t)$. The relative phase is obtained from the Fourier transformed coherent current $J^{coh}(\omega)$ at the spectral position of maximal current amplitude $|J^{coh}(\omega)|$. In Fig. 6(a) one can identify regions where the phase changes by about π, i.e., the initial direction of the alternating current changes when tuning the photon energy. The overall behavior of the peak-to-peak amplitude of J^{coh} shown in Fig. 6(b) is quite different than the photon energy dependence of J^{pop}, see Fig. 4. For example, whereas J^{pop}

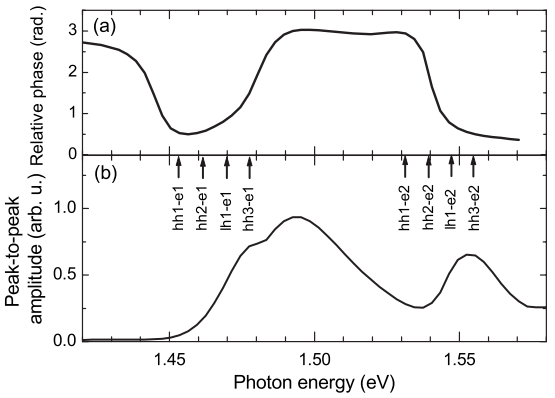

FIG. 6. Relative phase (a) and peak-to-peak amplitude (b) of the coherent current J^{coh} versus photon energy for a [110]-grown GaAs/$Al_{0.35}Ga_{0.65}As$ QW system with a 12-nm-wide well.

vanishes at certain spectral positions, J^{coh} is always finite when exciting above the band gap. Furthermore, the peak of J^{pop} at about 1.47 eV is not present in J^{coh} and the amplitude of J^{pop} is larger at 1.55 eV than at 1.5 eV which is opposite to the behavior of J^{coh}. Significant differences between the photon energy dependencies of J^{pop} and J^{coh} are to be expected since J^{coh} originates from intersubband coherences whereas J^{pop} is determined be electron populations, see Eqs. (10) and (11). To generate large intersubband coherences two optical transitions have to be excited and the subband splitting cannot be larger than the spectral width of the incident laser beam. Furthermore, significant optical matrix elements need to be present for the involved intersubband and intersubband transitions.

Next we analyze the influence of excitonic effects on the population current amplitude. For these calculations we use a thinner QW structure with a well width of 5 nm to obtain a stronger excitonic effect. Furthermore, the thinner QW has a larger splitting between the subband which allows us to reduce the number of subbands in our numerical calculations. We solve the multisubband SBE with excitonic effects including one conduction band (e1) and three valence subbands (hh1, hh2, and lh1), i.e., eight bands are considered since each one consists of two spin-split branches. The photon energy dependence of charge current computed with and without Coulomb interaction is shown by the solid line and the dashed line of Fig. 7, respectively. With Coulomb interaction J^{pop} is enhanced near and below the band gap. In particular, J^{pop} shows two peaks at $\hbar\omega=1.519$ and 1.554 eV, which correspond to excitation of the hh1 and lh1 excitonic resonances. These results demonstrate that in agreement with experimental findings[24] significant injection currents exist for excitation of exciton transitions. For higher photon energies the two lines shown in Fig. 7 approach each other, which confirms our assumption that it is allowed to neglect excitonic effects for excitation frequencies well above the band gap. It should be noted that both the solid and the dashed lines in Fig. 7 change sign at about 1.6 eV, i.e., excitonic effects do not inhibit the photon-energy-dependent direction reversal of the population charge current J^{pop}. Besides the population current discussed here, also a finite coherent current J^{coh} exists in the presence of excitonic effects. Because

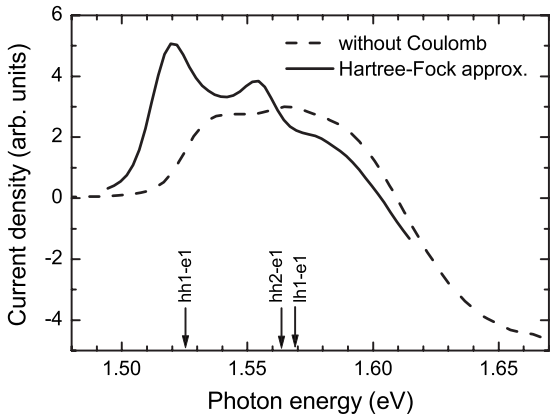

FIG. 7. Photon energy dependence of the population charge current J^{pop} at $t=100$ fs for a [110]-grown GaAs/$Al_{0.35}Ga_{0.65}As$ QW system with a 5-nm-wide well. Vertical arrows show the photon energies corresponding to interband transitions at the band edge.

of the rather large energy separation between the subbands for the 5-nm-wide QW considered here, the coherent current corresponds only to a very small part of the overall current since it is not effectively excited by the 150-fs-long incident laser beam.

2. [001]-grown QWs

To generate charge currents in QWs grown in the direction [001] oblique excitation is required.[8] The geometry of excitation is shown in Fig. 2(b) and the exciting light field is taken as

$$\mathbf{E}(t) = E_0 e^{-(t/\tau_L)^2} e^{i\omega t}(1, e^{i\phi}\cos\theta, e^{i\phi}\sin\theta) + \text{c.c.}, \quad (19)$$

where θ is the angle of incidence inside the QW medium. In the following calculations we use $\theta=-15°$. The optical excitation with a circularly polarized light field ($\phi=\pi/2$) results in a charge current flowing in the direction [010].

The photon-energy dependence of the population charge current J^{pop} for a [001]-grown QW is plotted in Fig. 8. The

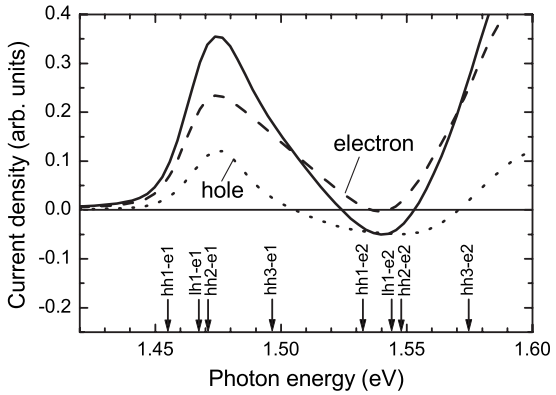

FIG. 8. Photon-energy dependence of the population charge current J^{pop} at $t=100$ fs for a [001]-grown GaAs/$Al_{0.35}Ga_{0.65}As$ QW system with a 12-nm-wide well. The vertical arrows highlight the photon energies that correspond to different interband transitions at $\mathbf{k}_\parallel=0$.

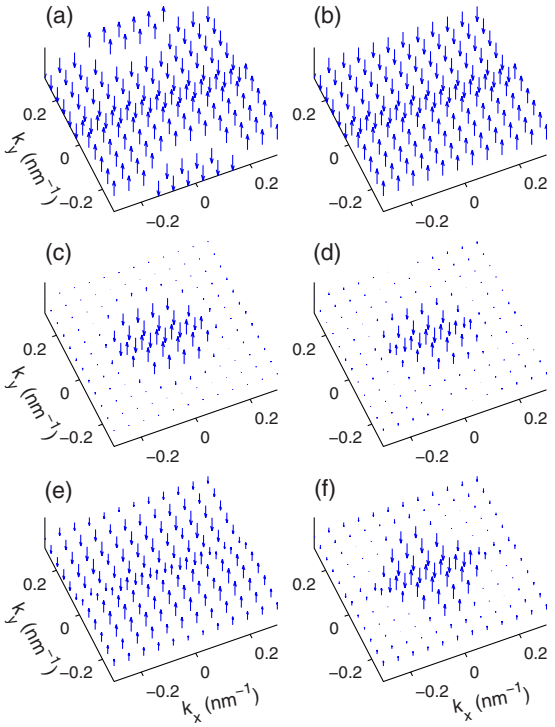

FIG. 9. (Color online) Orientation of the spin $\mathbf{\Sigma}_k^{\lambda\lambda}$ for the lower spin-split branch of the (a) e1 and the (b) e2 conduction bands and in the upper spin-split branch of the (c) hh1, (d) the hh2, (e) the lh1, and (f) the hh3 valence bands for a [110]-grown $GaAs/Al_{0.35}Ga_{0.65}As$ QW system with a 12-nm-wide well.

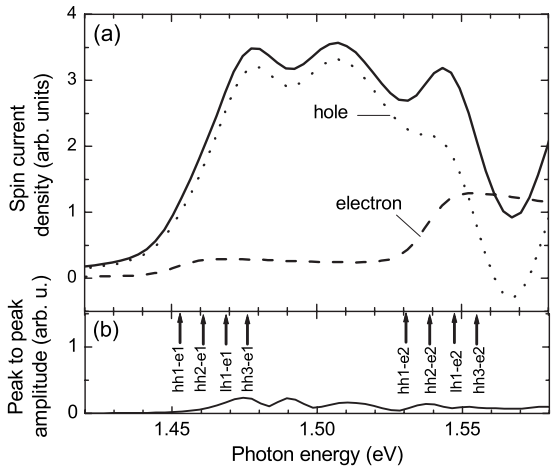

FIG. 10. (a) The dependence of the population spin current S^{pop} at $t=100$ fs and (b) peak-to-peak amplitude of the coherent spin current S^{coh} on the photon energy for a [110]-grown $GaAs/Al_{0.35}Ga_{0.65}As$ QW system with a 12-nm-wide well excited by circularly polarized pulses. In (a) besides the total current (solid line) also the electron (dashed line) and the hole (dotted line) contributions are shown. The vertical arrows highlight the photon energies that correspond to different interband transitions at $\mathbf{k}_\parallel=0$.

dashed, dotted, and solid lines represent the electron, the hole, and the total population charge currents, respectively. Similarly to the case of a [110]-grown QW, also for the [001]-grown QW the hole current contribution results in a reversal of the overall charge current direction as function of the photon energy. Since the spin-splitting of the hole subbands is smaller for the [001]-grown QW than for the [110]-grown QW, see Figs. 1(a) and 1(b), the relative importance of the hole current contribution is reduced and the current reversal is less pronounced.

B. Spin current

The expectation value of the spin of electron states calculated by Eqs. (14) and (15) for a [110]-grown $GaAs/Al_{0.35}Ga_{0.65}As$ QW system with a 12-nm-wide well is shown in Figs. 9(a)–9(f). Unlike for the [001]-grown QWs, the spin orientation of electrons and holes for [110]-grown QWs is always perpendicular to the plane of the QW.[35,36] This makes [110]-grown QWs a highly interesting system for spin current investigations.[19] Figures 9(a) and 9(b) represent Σ_k^{cc} in the lower spin-split branches of the e1 and the e2 conduction bands while Figs. 9(c)–9(f) displays Σ_k^{vv} in the upper spin-split branch of the hh1, the hh2, the lh1, and the hh3 valence bands, respectively. The direction and length of arrows describe the direction and magnitude of the spins in k space. In the conduction bands, the magnitude is 1/2 and only the direction changes when subbands cross. For the valence bands, due to the mixing of heavy-hole and light-hole bands, the magnitude of spins takes a value between 0 and 3/2 depending on the wave vector $\mathbf{k}_\parallel$. In particular for the hh subbands, the magnitude of the spin decreases at larger k values due to band mixing.

In the following we discuss numerical results on the spin current injection by circularly polarized pulses. The computed spin current consists of spins that are aligned along the z axis and flow in the direction $y=[\bar{1}10]$. The photon-energy dependence of the population spin current S^{pop} at $t=100$ fs is shown as the thick solid line in Fig. 10(a). The dashed and dotted lines show the contributions to S^{pop} by electrons and holes separately. Since the magnitude of the spin as well as the spin-splitting are larger for holes than for electrons the spin current is dominated by the holes. The higher complexity of the photon energy dependence of the spin current of the holes compared to that of the electrons is due to valence band mixing. For illustration, the spin distribution in k space calculated as $\Sigma_{z,k}^{\lambda\lambda}n_k^{\lambda\lambda}$, i.e., spin projection times the population, for two conduction bands (e1, e2) and four valence bands (hh1, hh2, lh1, and hh3) is shown in Figs. 11(a)–11(f), respectively. Figure 11 clearly shows a almost circularly symmetric distribution of the electron spin and a pronounced asymmetry of the hole spin distributions. The arrows denote the direction and magnitude of the spin current in each band. As for the charge current[31] also the spin current contributions from different valence subband point into opposite direction.

The dependence of the peak to peak amplitude of the coherent spin current S^{coh} on photon energy is shown as the thin solid line in Fig. 10(b). As for J^{coh}, also for S^{coh} for the QW structures and excitation conditions used here, the electron contribution is negligible and the overall coherent current is dominated by hole intersubband coherences. S^{coh} shows an interesting photon energy dependence with some relative maxima. As for the coherent charge current J^{coh} also the coherent spin current S^{coh} depends on the optical matrix

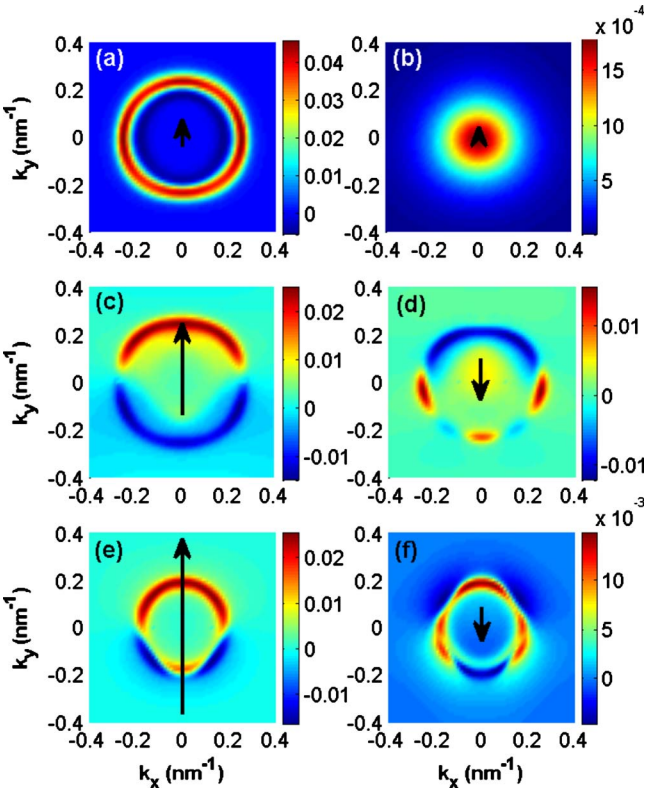

FIG. 11. (Color online) k-space distribution of the mean value of the z component of the spin $\Sigma_{z,k}^{\lambda\lambda} n_k^{\lambda\lambda}$ in the conduction subbands (a) e1 and (b) e2, and in the valence subbands (c) hh1, (d) hh2, (e) lh1, and (f) hh3 at time $t=100$ fs for a [110]-grown $GaAs/Al_{0.35}Ga_{0.65}As$ QW system with a 12-nm-wide well. The circularly polarized excitation pulses have a photon energy of $\hbar\omega = 1.501$ eV, a duration of $\tau_L = 150$ fs, and an amplitude of $E_0 = 4.5 \times 10^4$ V/cm.

elements for the involved intersubband and intersubband transitions. Additionally, S^{coh} is also proportional to $\Sigma_{z,k}^{\lambda\lambda'}$ which for the holes has a complex k dependence. It is the combination of all these effects that results in the computed frequency dependence of S^{coh}.

IV. CONCLUSION

A general and microscopic theory that is capable of describing the generation and ultrafast dynamics of charge and spin injection currents in semiconductor QW structures has been developed and evaluated for a $GaAs/Al_{0.35}Ga_{0.65}As$ QW systems grown in [110] and [001] directions. It is shown that the direction reversal of the population charge current J^{pop} as function of the photon energy that has recently been described for [110]-grown QWs (Ref. 31) also exists in [001]-grown systems. Thus this interesting effect is not restricted to a single special growth direction. For [110]-grown QWs we have computed and compared the frequency dependence of the population and the coherent charge currents, i.e., J^{pop} and J^{coh}. Due to the differences between the photoexcitations of populations and intersubband coherences and the involved matrix elements, J^{pop} and J^{coh} show a very different frequency dependence. Thus to a great extend one can tune both current contributions separately by changing the central frequency of the incident laser pulse.

Including excitonic effects in our calculations of J^{pop} we find an enhanced current generation for excitation of the hh- and lh-exciton resonances. Our calculations confirm that excitonic effects get weaker for higher excitation frequencies. Furthermore, they do not inhibit the direction reversal of the population charge current J^{pop} as function of the photon energy.

Due to the coupling among the valence bands, the direction and magnitude of the heavy-hole and light-hole spins vary strongly in k space for the considered [110]-grown QW structure. This rich k dependence leads to a nontrivial photon energy dependence of the population S^{pop} and coherent spin currents S^{coh}. It is shown that similarly to the population charge current also the population spin current contributions from different valence subbands flow into opposite directions.

ACKNOWLEDGMENTS

We thank M. Bieler, B. Pasenow, S. W. Koch, and J. E. Sipe for useful discussions. The work is supported by the Deutsche Forschungsgemeinschaft (DFG) through ME 1916/2, FO 637/1, and GRK 1464.

[1] B. I. Sturman and V. M. Fridkin, *The Photovoltaic and Photorefractive Effects in Noncentrosymmetric Materials* (Gordon and Breach, Philadelphia, 1992).
[2] E. Dupont, P. B. Corkum, H. C. Liu, M. Buchanan, and Z. R. Wasilewski, Phys. Rev. Lett. **74**, 3596 (1995).
[3] R. Atanasov, A. Haché, J. L. P. Hughes, H. M. van Driel, and J. E. Sipe, Phys. Rev. Lett. **76**, 1703 (1996).
[4] A. Haché, Y. Kostoulas, R. Atanasov, J. L. P. Hughes, J. E. Sipe, and H. M. van Driel, Phys. Rev. Lett. **78**, 306 (1997).
[5] P. Král, J. Phys.: Condens. Matter **12**, 4851 (2000).
[6] J. E. Sipe and A. I. Shkrebtii, Phys. Rev. B **61**, 5337 (2000).
[7] R. D. R. Bhat and J. E. Sipe, Phys. Rev. Lett. **85**, 5432 (2000).
[8] S. D. Ganichev, E. L. Ivchenko, S. N. Danilov, J. Eroms, W. Wegscheider, D. Weiss, and W. Prettl, Phys. Rev. Lett. **86**, 4358 (2001).
[9] S. D. Ganichev, U. Rössler, W. Prettl, E. L. Ivchenko, V. V. Bel'kov, R. Neumann, K. Brunner, and G. Abstreiter, Phys. Rev. B **66**, 075328 (2002).
[10] S. D. Ganichev and W. Prettl, J. Phys.: Condens. Matter **15**, R935 (2003).
[11] L. E. Golub, Phys. Rev. B **67**, 235320 (2003).
[12] M. J. Stevens, A. L. Smirl, R. D. R. Bhat, A. Najmaie, J. E. Sipe, and H. M. van Driel, Phys. Rev. Lett. **90**, 136603 (2003).
[13] J. Hübner, W. W. Rühle, M. Klude, D. Hommel, R. D. R. Bhat,

J. E. Sipe, and H. M. van Driel, Phys. Rev. Lett. **90**, 216601 (2003).
[14] D. H. Marti, M.-A. Dupertuis, and B. Deveaud, Phys. Rev. B **69**, 035335 (2004).
[15] D. H. Marti, M.-A. Dupertuis, and B. Deveaud, Phys. Rev. B **72**, 075357 (2005).
[16] R. D. R. Bhat and J. E. Sipe, Phys. Rev. B **72**, 075205 (2005).
[17] H. T. Duc, T. Meier, and S. W. Koch, Phys. Rev. Lett. **95**, 086606 (2005).
[18] R. D. R. Bhat, F. Nastos, A. Najmaie, and J. E. Sipe, Phys. Rev. Lett. **94**, 096603 (2005).
[19] H. Zhao, X. Pan, A. L. Smirl, R. D. R. Bhat, A. Najmaie, J. E. Sipe, and H. M. van Driel, Phys. Rev. B **72**, 201302(R) (2005).
[20] H. T. Duc, Q. T. Vu, T. Meier, H. Haug, and S. W. Koch, Phys. Rev. B **74**, 165328 (2006).
[21] F. Nastos and J. E. Sipe, Phys. Rev. B **74**, 035201 (2006).
[22] N. Laman, M. Bieler, and H. M. van Driel, J. Appl. Phys. **98**, 103507 (2005).
[23] M. Bieler, K. Pierz, and U. Siegner, J. Appl. Phys. **100**, 083710 (2006).
[24] M. Bieler, K. Pierz, U. Siegner, and P. Dawson, Phys. Rev. B **73**, 241312(R) (2006).
[25] L. Costa, M. Betz, M. Spasenovic, A. D. Bristow, and H. M. van Driel, Nat. Phys. **3**, 632 (2007).
[26] J. Güdde, M. Rohleder, T. Meier, S. W. Koch, and U. Höfer, Science **318**, 1287 (2007).
[27] S. Giglberger, L. E. Golub, V. V. Bel'kov, S. N. Danilov, D. Schuh, C. Gerl, F. Rohlfing, J. Stahl, W. Wegscheider, D. Weiss, W. Prettl, and S. D. Ganichev, Phys. Rev. B **75**, 035327 (2007).
[28] B. Pasenow, H. T. Duc, T. Meier, and S. W. Koch, Solid State Commun. **145**, 61 (2008).
[29] M. Spasenović, M. Betz, L. Costa, and H. M. van Driel, Phys. Rev. B **77**, 085201 (2008).
[30] C. Sames, J. M. Menard, M. Betz, A. L. Smirl, and H. M. van Driel, Phys. Rev. B **79**, 045208 (2009).
[31] S. Priyadarshi, A. M. Racu, K. Pierz, U. Siegner, M. Bieler, H. T. Duc, J. Förstner, and T. Meier, Phys. Rev. Lett. **104**, 217401 (2010).
[32] H. Mayer and U. Rössler, Phys. Rev. B **44**, 9048 (1991).
[33] P. von Allmen, Phys. Rev. B **46**, 15382 (1992).
[34] P. Pfeffer and W. Zawadzki, Phys. Rev. B **52**, R14332 (1995).
[35] R. Winkler, *Spin-orbit Coupling Effects in Two-Dimensional Electron and Hole Systems* (Springer, Berlin, 2003).
[36] R. Winkler, Phys. Rev. B **69**, 045317 (2004).
[37] M. Bieler, K. Pierz, U. Siegner, P. Dawson, H. T. Duc, J. Förstner, and T. Meier, Proc. SPIE **7214**, 721404 (2009).
[38] H. T. Duc, J. Förstner, and T. Meier, Proc. SPIE **7600**, 76000S (2010).
[39] H. Haug and S. W. Koch, *Quantum Theory of the Optical and Electronic Properties of Semiconductors*, 4th ed. (World Scientific, Singapore, 2004).
[40] W. Schäfer and M. Wegener, *Semiconductor Optics and Transport Phenomena* (Springer, Berlin, 2002).
[41] J. J. Sakurai, *Modern Quantum Mechanics* (Addison-Wesley, London, 1994).
[42] A. Twardowski and C. Hermann, Phys. Rev. B **35**, 8144 (1987).